Metallomics

Integrated biometal science

www.rsc.org/metallomics

Volume 5 | Number 10 | October 2013 | Pages 1329–1460

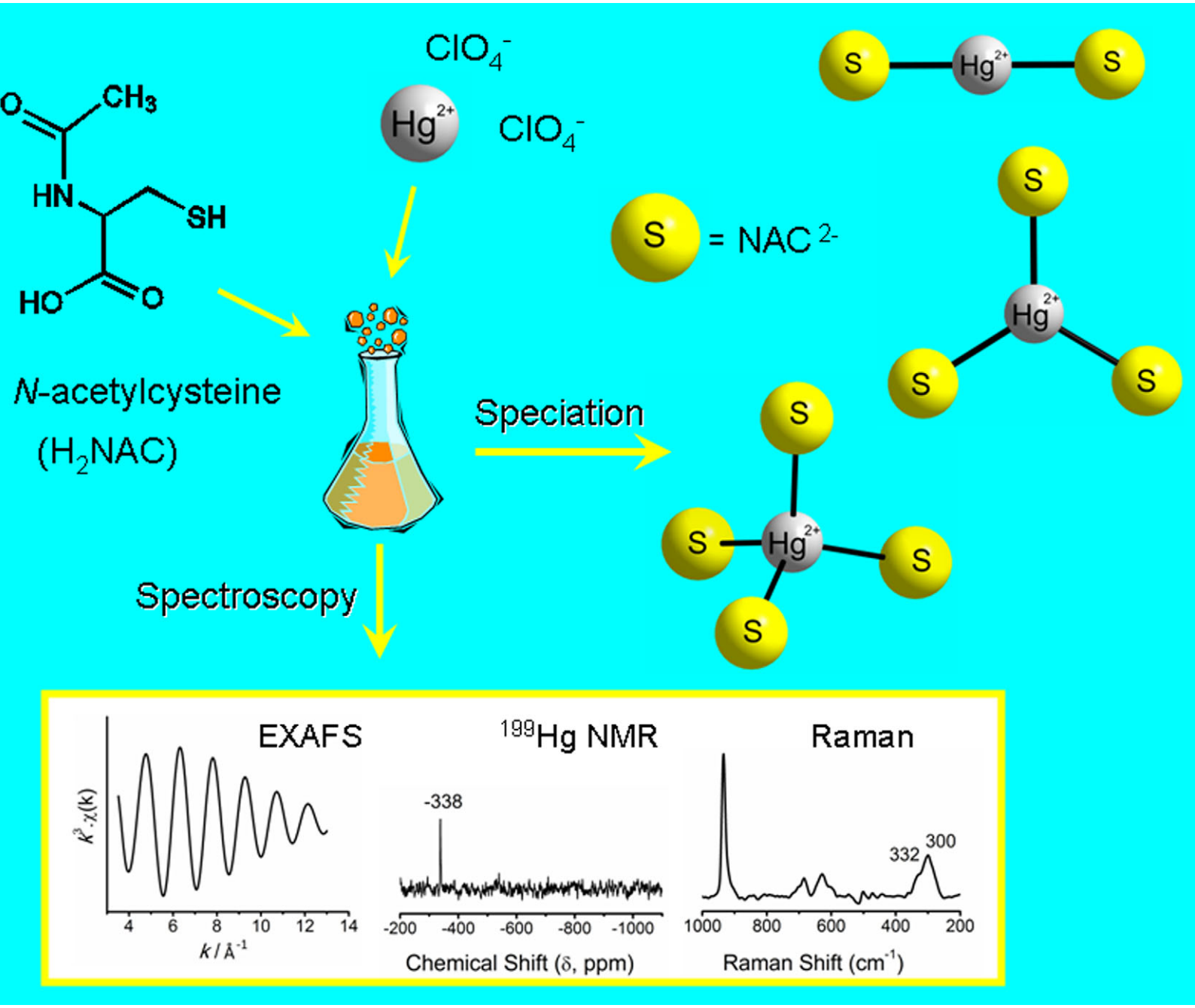

ISSN 1756-5901

RSC Publishing

PAPER

Farideh Jalilehvand *et al.*

Mercury(II) complex formation with *N*-acetylcysteine

Indexed in MEDLINE!

Metallomics

RSC Publishing

PAPER

View Article Online
View Journal | View Issue

Mercury(II) complex formation with *N*-acetylcysteine†

Cite this: *Metallomics*, 2013, **5**, 1368

Farideh Jalilehvand,* Karnjit Parmar and Stephen Zielke

Received 8th June 2013,
Accepted 30th July 2013

DOI: 10.1039/c3mt00173c

www.rsc.org/metallomics

N-Acetylcysteine (H_2NAC) is a potent antioxidant, a precursor for cysteine and glutathione, and a potential antidote against certain metal ions such as cadmium and mercury. Little is known about the structural aspects of complexes formed between Hg(II) and *N*-acetylcysteine, despite many biological tests on its ability to bind to organic and inorganic mercury, and a few reports on formation constants for $Hg(NAC)_n$ (n = 1–3) complexes. We have combined several techniques, including Hg L_3-edge EXAFS (extended X-ray absorption fine structure), ^{199}Hg NMR and Raman spectroscopy, to investigate the nature and structure of Hg(II) *N*-acetylcysteine complexes formed in aqueous solution at pH 7.5 and 10.5. To allow measurements on the same samples, rather concentrated solutions containing $C_{Hg(II)}$ = 0.1 M and variable $H_2NAC/Hg(II)$ mole ratios = 2.0–10.0 were used. At physiological pH, $Hg(NAC)_2^{2-}$ and $Hg(NAC)_3^{4-}$ complexes form, while in ligand excess and at alkaline pH ($H_2NAC/Hg(II)$ > 4), a novel tetrathiolate species $Hg(NAC)_4^{6-}$ dominates. Comparison between the Hg(II) complex formation with cysteine, penicillamine and *N*-acetylcysteine in alkaline aqueous solution has been made to elucidate the influence of the blocked amino group of *N*-acetylcysteine.

Introduction

Human exposure to mercury can occur through different sources, such as industrial products (batteries, thermometers and fluorescent lamps), contaminated seafood and agricultural products, dental amalgam and thimerosal, a preserving agent used in some vaccines.[1] Mercury compounds are classified into inorganic (metallic Hg^0 and Hg_2^{2+}/Hg^{2+} salts) and organomercury (*e.g.* CH_3Hg^+) compounds, which can be partially metabolized into inorganic mercury in the body.[2] The toxicity depends on the chemical/molecular form.[2,3] Mercury can influence the central nervous system and accumulates mainly in kidneys.[1,2] X-ray fluorescence imaging of human brain tissues following poisoning with methylmercury or environmental exposure has shown different levels of three forms of mercury: insoluble HgSe nanoparticles as non-bioavailable and non-toxic form, and thiolate-bound methylmercury (CH_3Hg–SR) and inorganic mercury $Hg(SR)_2$ as mobile, toxic forms.[4]

Different chelating agents are currently in clinical use for mercury detoxification with 2,3-dimercapto-1-propanesulfonic acid (DMPS) and 2,3-dimercaptosuccinic acid (*meso*-DMSA) being the most efficient drugs, and also D-penicillamine (Scheme 1), *N*-acetyl-D-penicillamine and 2,3-dimercapto-1-propanol (BAL).[5,6] Animal tests have shown that *N*-acetylcysteine, a potent antioxidant and a precursor of L-cysteine and glutathione,[7] is capable of acting as an antidote for certain heavy metal ions, including inorganic and organic mercury, cadmium and chromium.[5] *N*-Acetylcysteine (Scheme 1) has been widely used as an antidote to acetaminophen overdose, but has also multiple other clinical applications, *e.g.* treatment of cancer, HIV infections, and cardiovascular diseases.[8,9] According to the Toxic Exposure database compiled by the American Association of Poison Control Centers, *N*-acetylcysteine is the most common emergency antidote.[6,10]

Oral administration of *N*-acetylcysteine (H_2NAC) accelerated urinary excretion of methylmercury in mice,[11] and it was suggested that *N*-acetylcysteine could be more effective than DMPS or D-penicillamine for enhancing renal excretion of methylmercury.[12] However, there are conflicting reports about $HgCl_2$ excretion upon *N*-acetylcysteine treatment.[11,13,14] Recently, an *in vitro* study on detoxification of mercury species from human blood was performed using common antidotes such as H_2NAC. Plasma surrogate samples were spiked with

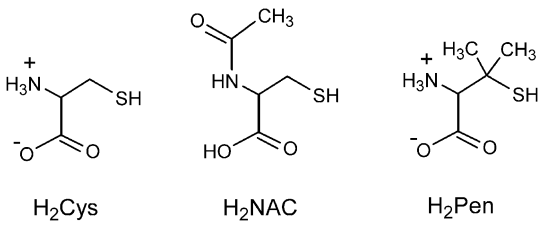

Scheme 1 The structures of *N*-acetylcysteine (H_2NAC), and zwitterionic forms of cysteine (H_2Cys), and penicillamine (H_2Pen).

Department of Chemistry, University of Calgary, Calgary, Alberta, T2N 1N4, Canada. E-mail: faridehj@ucalgary.ca

† Electronic supplementary information (ESI) available. See DOI: 10.1039/c3mt00173c

CH_3Hg^+ and Hg(II), followed by addition of H_2NAC. Liquid chromatography coupled with mass spectrometry (ICP-MS or ESI-TOF-MS) showed that the dominating species were $CH_3Hg(NAC)$ and $Hg(NAC)_2$, respectively; no Hg–glutathione (GSH) adduct was observed.[15] Therefore, it was proposed that these complexes reduce the mercury level in the body, and that Hg–GSH adducts that are formed under physiological conditions easily decompose in the presence of antidotes like H_2NAC, releasing glutathione. Other studies suggest that the GSH synthesis is promoted, and the level of non-protein thiols increases, when *N*-acetylcysteine is used as treatment for $HgCl_2$ toxicity.[14,16,17] Meanwhile it has been shown that both $CH_3Hg(NAC)$ and $Hg(NAC)_2$ complexes are transportable *in vivo*.[18,19] Brandão *et al.* observed that the renal Na^+, K^+-ATPase activity was inhibited in mice exposed to $HgCl_2$ and *N*-acetylcysteine (or DMPS), and concluded that Hg(II) complexes with *N*-acetylcysteine (or DMPS) may even increase the mercury renal uptake and enhance Hg toxicity.[20] They also reported *in vitro* inhibition of δ-aminolevulinate dehydratase (δ-ALA-D) activity by $HgCl_2$ + *N*-acetylcysteine, suggesting that the resulting Hg(II)–NAC complex could oxidize the thiol group in δ-ALA-D and also in Na^+, K^+-ATPase enzymes, making them inactive.[21] The NAC–Hg–NAC complex has been studied by mass spectrometry.[22]

N-Acetylcysteine (H_2NAC) has two potential coordination sites: the carboxyl (–COOH) and the thiol (–SH) groups, with acid dissociation constants $pK_1 = 3.31$ and $pK_2 = 9.85$,[23] (or 3.01 and 9.69 at 25 °C and $I = 0.5$ M $NaClO_4$),[24] respectively. Fig. S1 (ESI†) displays the pH dependence of different protonated forms of *N*-acetylcysteine. Stability constants ($\log\beta$) have been reported for the complexes $Hg(HNAC)_2$ 47.83, $Hg(NAC)(HNAC)^-$ 45.37, $Hg(NAC)_2^{2-}$ 41.81 and $Hg(NAC)_3^{4-}$ 44.37 (25 °C and $I = 0.5$ M $NaClO_4$).[24] These values differ somewhat from the successive formation constants ($\log K$) reported earlier for Hg(NAC) 38.4 and $Hg(NAC)_2^{2-}$ 7.2.[25]

The $Hg(NAC)_3^{4-}$ complex only formed at high free ligand concentration [NAC^{2-}], with the stability constant ratio for $Hg(NAC)_3^{4-}$ and $Hg(NAC)_2^{2-}$ determined to be: $\log\{[Hg(NAC)_3^{4-}]/[Hg(NAC)_2^{2-}][NAC^{2-}]\} = 2.56$. However, there is no structural information available about Hg(II) complexes with *N*-acetylcysteine. Fig. S2 (ESI†) displays calculated distribution diagrams for Hg(II) *N*-acetylcysteine complexes as a function of the total H_2NAC concentration for the conditions of the current study: $C_{Hg(II)}$ = 0.1 M, pH = 7.5 and 10.5.

In the past few years, our group has investigated mercury(II) complex formation with cysteine, D-penicillamine and glutathione in aqueous solution using ^{199}Hg NMR, Raman and extended X-ray absorption fine structure (EXAFS) spectroscopic techniques.[26–29] The purpose of our current study is to structurally characterize Hg(II) *N*-acetylcysteine complexes in aqueous solution (pH = 7.5 and 10.5), and to explore the influence of the blocked amino group of *N*-acetylcysteine, in comparison with the above ligands, on the nature of Hg(II) complexes formed. In alkaline media the thiol group of the free ligand is deprotonated, providing high concentration of free thiolate and enhancing the formation of higher Hg(II)–NAC complexes.

Experimental section

Sample preparation

All samples were synthesized and handled under an argon atmosphere using O_2-free water/D_2O, to avoid the formation of disulfides. Degassing was performed by boiling water or D_2O and then bubbling argon through it while cooling. *N*-Acetylcysteine, mercury(II) perchlorate hydrate $Hg(ClO_4)_2{\cdot}0.8H_2O$ (analyzed by Sigma Aldrich) and sodium hydroxide were used as obtained from Sigma Aldrich. The pH of solutions was monitored using a Corning Semi-Micro electrode, calibrated with standard buffers.

The solutions were prepared by dissolving *N*-acetylcysteine (1.0–5.0 mmol) in ~3.5 mL oxygen-free water and D_2O, adding $Hg(ClO_4)_2{\cdot}0.8H_2O$ (0.5 mmol) while stirring. The white precipitate initially formed gradually dissolved. Two sets of aqueous solutions A1–F1 (pH ~ 7.5) and A2–F2 (pH ~ 10.5) were prepared, containing different H_2NAC/Hg(II) mole ratios and 10% D_2O to enable ^{199}Hg NMR, Raman and EXAFS measurements on the same solutions (Table 1). The pH of solutions was adjusted by dropwise addition of 6 M NaOH, and their total volumes were set to 5.0 mL.

Nuclear Magnetic Resonance (NMR) and Raman spectroscopy

A Bruker Avance DRX-400 spectrometer equipped with a 5 mm broadband probe (BB5) was used to measure ^{199}Hg NMR spectra of solutions A1–F1 and A2–F2 at a resonance frequency of 71.49 MHz. The ^{199}Hg chemical shift was externally calibrated by means of a saturated solution of $HgCl_2$ in D_2O, resonating at −1550 ppm (with $Hg(CH_3)_2$ at 0 ppm).[30,31] The NMR data were collected at room temperature using a 30° pulse and zgdc30 pulse program with a sweep width of 1200 ppm and proton decoupling. The total number of averaged scans was: 40 171 (A1), 100 009 (B1), 140 936 (C1), 250 000 (D1), 294 692 (E1), 181 308 (F1), 73 431 (A2), 78 889 (B2), 139 791 (C2), 133 377 (D2), 5326 (E2) and 7655 (F2), with 1.0 s delay time between the scans.

The Raman spectra were measured by exposing the solutions in closed vials to the 1064 nm line from a YAG laser at 500 mW, using a Bruker RAM II FT-Raman spectrometer equipped with a liquid N_2 cooled Ge detector. About 4000 scans were co-added in the range of 100–4000 cm^{-1} with 4 cm^{-1} resolution. Baseline correction was performed using the OPUS program, subtracting the bands from a vial containing water. A 9-point Savitzky–Golay filter was used for smoothing.

Table 1 Composition of the Hg(II) *N*-acetylcysteine solutions[a]

Solution (pH ~ 7.5)	H_2NAC/Hg^{2+} mole ratio	$[Hg^{2+}]_{tot}$	$[H_2NAC]_{tot}$	Solution (pH ~ 10.5)
A1	2.0	100	200	A2
B1	3.0	100	300	B2
C1	4.0	100	400	C2
D1	5.0	100	500	D2
E1	8.0	100	800	E2
F1	10.0	100	1000	F2

[a] Concentrations in mM.

EXAFS data collection

Hg L_3-edge X-ray absorption spectra of the solutions were measured at BL 7-3 at the Stanford Synchrotron Radiation Lightsource (SSRL) under dedicated conditions of 3.0 GeV and 350 mA. The solutions were loaded under an argon atmosphere into a 5 mm Teflon spacer with 5 μm polypropylene windows, and exposed to fully tuned radiation (I_0) with 1 × 1 mm^2 beam size. Higher harmonics were discarded by a Rh-coated mirror after the Si(220) double crystal monochromator. For each solution, 2–3 scans were measured at room temperature in fluorescence mode, using a PIPS solid state detector to monitor Hg L_α radiation, and a germanium filter (Ge-3) to reduce the scattered radiation. A sample of $HgCl_2$ mixed with boron nitride was placed between the second (I_1) and third (I_2) ion chambers for energy calibration, setting its first inflection point at 12 284.0 eV. The ion chambers placed before (I_0) and after (I_1) the sample position were filled with nitrogen, and I_2 with argon.

EXAFS data analysis

For each sample, the individual scans were compared and their energy scale was calibrated, prior to averaging using the EXAFSPAK suite of programs.[32] The EXAFS oscillations were extracted by means of the WinXAS 3.1 program,[33] subtracting a first-order polynomial background over the pre-edge region, followed by normalization over the edge step. Conversion of the energy scale to k-space, $k = [(8\pi^2 m_e/h^2)(E - E_0)]^{1/2}$, was performed using a threshold energy of E_0 = 12 284.9–12 285.2 eV (the 1st inflection point in the absorption spectra of the solutions). The atomic background contribution in the post-edge region was removed using a seven segment cubic spline.

Simulated EXAFS oscillation, $\chi(k)$, was modeled based on the following expression:

$$\chi(k) = \sum_i \frac{N_i {S_0}^2}{kR_i^2} |f_{\text{eff}}(k)|_i \exp\left(-2k^2\sigma_i^2\right) \times \exp[-2R_i/\Lambda(k)] \sin\left[2kR_i + \phi_{ij}(k)\right]$$

where N_i is the number of backscattering atoms at the mean distance R_i from the absorber in the ith shell; ${\sigma_i}^2$ is the Debye–Waller parameter related to the mean-square variation in a Gaussian distribution of distances around R_i; k is the scattering variable; ${S_0}^2$ is the amplitude reduction factor; $|f_{\text{eff}}(k)|_i$ is the effective amplitude function; $\phi_{ij}(k)$ is the total phase-shift of the absorber–scatterer pair, and $\lambda(k)$ is the photoelectron mean free path.

The effective amplitude, phase shift and the mean free path functions for Hg–S and potential Hg–O scattering paths were obtained by performing FEFF 8.1 *ab initio* calculations,[34,35] using the atomic coordinates from the $Hg(SCH_2CH_2NH_2)_2$ crystal structure,[36] where cysteamine is coordinated to the Hg(II) ion in a *S*,*N*-bidentate mode. Structural parameters for the Hg–S scattering path in solutions A1–F1 and A2–F2 were obtained by least square refinements of the theoretical model $\chi(k)$ to the k^3-weighted experimental EXAFS oscillation over the k-range of 3.5–15.8 $Å^{-1}$ (13.0 $Å^{-1}$ for F2), fixing ${S_0}^2$ at 0.9,[26] and allowing R, N, σ^2 and ΔE_0 to float. The ΔE_0 value varied between 10.0–11.0 eV for solutions A1, B1, A2, B2 and D2–F2, and between 8.7–9.8 for the other solutions. The accuracy of the mean bond distances R is estimated to be ±0.02 Å (for the linear complex ±0.01 Å), and that of the average coordination numbers N within ±20%.

EXAFS linear combination fitting

To estimate the relative amounts of two-, three- and four-coordinated mercury(II) *N*-acetylcysteine complexes in the solutions, the k^3-weighted experimental EXAFS oscillations for solutions A1–F1 and A2–F2 were fitted to linear combinations of theoretical EXAFS oscillations for the $Hg(NAC)_2^{2-}$, $Hg(NAC)_3^{4-}$ and $Hg(NAC)_4^{6-}$ species, which were simulated by means of the WinXAS 3.1 and FEFF 8.1 programs, using the parameters shown in Table 2 for the single-scattering Hg–S path.[26–29] The ΔE_0 was fixed at 11.0 eV; the Hg–S bond distance and σ^2 values for the $Hg(NAC)_2^{2-}$ complex were chosen to be 2.33 Å and 0.003 $Å^2$, respectively, similar to the corresponding refined values obtained for solutions A1 and A2. The Hg–S distances for the other two species were varied within the ranges reported for crystalline HgS_3 and HgS_4 complexes.[27] For the linear combination fitting procedure, the DATFIT program in the EXAFSPAK package was used. The best fits with minimum residuals over the k-range = 2.8–15.7 $Å^{-1}$ were obtained for the mean Hg–S distances 2.42 and 2.52–2.53 Å, with Debye–Waller parameters σ^2 = 0.004–0.005 and 0.007 $Å^2$ for the tri-thiolate $Hg(NAC)_3^{4-}$ and tetra-thiolate $Hg(NAC)_4^{6-}$ complexes, respectively (see Fig. S3a and b, ESI†). These Debye–Waller parameters were also supported by FEFF 8.1 calculations based on the experimental Raman Hg–S symmetric stretching frequencies for $Hg(NAC)_2^{2-}$ (332 cm^{-1} in the spectra of solutions A1 and A2), $Hg(NAC)_3^{4-}$ (300 cm^{-1} in the spectra of solutions B2–D2), and $Hg(SPh)_4^{2-}$ (179 cm^{-1}), with corresponding harmonic force constants of 180.0, 146.6 and 52.2 N m^{-1} for an assumed ligand mass equal to an S atom, resulting in σ^2 values of 0.0027, 0.0033 and 0.0084 $Å^2$ for $Hg(NAC)_2^{2-}$, $Hg(NAC)_3^{4-}$ and $Hg(NAC)_4^{6-}$ complexes, respectively.

Results

X-ray absorption spectroscopy

Hg L_3-edge EXAFS spectra and corresponding least squares curve-fitting results for mercury(II) *N*-acetylcysteine solutions at both physiological (A1–F1) and alkaline (A2–F2) pH are shown in Fig. 1 and Table 3. The single Fourier-transform (FT) peak corresponding to the Hg–S scattering shows a gradual

Table 2 Parameters used to model EXAFS spectra of $Hg(NAC)_n$ species[a]

Species	N	$R_{\text{Hg–S}}$ (Å)	$\sigma^2 \times 10^3$ ($Å^2$)
$Hg(NAC)_2^{2-}$	2*f*	2.33*f* [2.33]	3*f* [3]
$Hg(NAC)_3^{4-}$	3*f*	2.42–2.45 [2.42]	4–7 [4–5]
$Hg(NAC)_4^{6-}$	4*f*	2.52–2.54 [2.52–2.53]	7–9 [7]

[a] ΔE_0 and ${S_0}^2$ values were fixed at 11.0 eV and 0.9 eV, respectively. Best fits were obtained using values in brackets (*f* = fixed value).

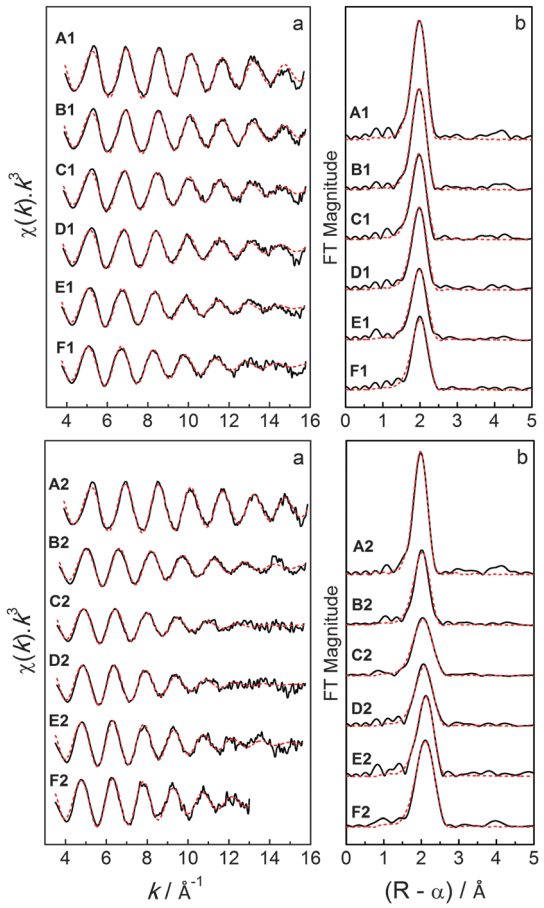

Fig. 1 (a) Hg L_3-edge EXAFS spectra and (b) the corresponding Fourier-transforms of Hg(II) *N*-acetylcysteine solutions at physiological (A1–F1) and alkaline (A2–F2) pH. Least-squares curve-fitting results are shown in Table 3 (exp. ——; fit – – –).

shift to higher distances as the ligand concentration increases, with the mean Hg–S distance changing from 2.33 ± 0.01 Å in solutions A1 and A2 containing C_{H_2NAC} = 0.2 M, to 2.39 and 2.52 ± 0.02 Å for solutions F1 and F2, respectively, both containing C_{H_2NAC} = 1.0 M. Simultaneously the relative FT peak intensity decreases from A1 to F1, and from A2 to D2, and then gains intensity again from D2 to F2. This intensity variation is due to a gradual increase in the Hg–S coordination number (N), counteracted by an increasing mean Debye–Waller parameter (σ^2) for solutions B1–F1 and B2–D2.

The mean Hg–S distances obtained for Hg(II) *N*-acetylcysteine solutions based on the EXAFS data analysis in Table 3 can be compared with the average crystallographic Hg–S distances in Hg(II) thiolate complexes: HgS_2 (2.34 ± 0.02 Å), HgS_3 (2.44 ± 0.04 Å) and HgS_4 (2.54 ± 0.02 Å).[27] The increasing σ^2 values (Table 3) are consistent with the higher coordination numbers, with an additional contribution from the distribution of Hg–S bond distances in a mixture of Hg(II)-thiolate species.

The experimental EXAFS spectra of solutions B1–F1 and B2–F2 were fitted to linear combinations of simulated EXAFS oscillations of HgS_2, HgS_3 and HgS_4 cores. The best fits were obtained assuming the Hg–S bond distances of 2.33, 2.42, 2.52–2.53 Å and corresponding σ^2 values of 0.003, 0.004–0.005 and 0.007 $Å^2$ for the $Hg(NAC)_2^{2-}$, $Hg(NAC)_3^{4-}$ and $Hg(NAC)_4^{6-}$ complexes, respectively (Table 2). Using this method, we could roughly estimate (with accuracy ±10–15%) the relative amounts of these complexes in the solutions B1–F1 and B2–F2 (see Table 4 and Table S1, ESI†).

Raman spectroscopy

Raman spectra of the Hg(II) *N*-acetylcysteine solutions are shown in Fig. 2. The peaks at 934 and 629 cm^{-1} correspond to Cl–O symmetric stretching and antisymmetric bending modes of ClO_4^-, respectively.[37] For solutions A1 (pH 7.5) and A2 (pH 10.5), the distinct Raman band at 332 cm^{-1} can be attributed to the symmetric S–Hg–S stretching in the linear $Hg(NAC)_2^{2-}$ complex.[30] For the $Hg(Cys)_2^{2-}$ complex, ν_{sym}(S–Hg–S) occurred at 334 cm^{-1}.[26] In the Raman spectra of solutions B1–F1 (pH 7.5), the intensity of this band gradually reduces, indicating decreasing concentration of the $Hg(NAC)_2^{2-}$ complex when the total ligand concentration increases, while the new peak at ~300 cm^{-1}, which grows in intensity, can be assigned as the Hg–S stretching in the tri-thiolate $Hg(NAC)_3^{4-}$ complex. For solution B2 (pH 10.5), the band at 332 cm^{-1} appears as a shoulder relative to the peak at 300 cm^{-1}, and then disappears in the spectra of solutions C2–F2 (pH 10.5). The peak area for the 332 cm^{-1} band could in principle be used to estimate the amount of the $Hg(NAC)_2^{2-}$ complex, when using a proper internal calibration such as the perchlorate ν_{sym}(Cl–O) band.[26] However, in the present study, the few drops of $HClO_4$ used for adjusting the pH of some solutions made the band at

Table 3 Structural parameters derived from EXAFS least-squares curve fitting for the Hg(II) *N*-acetylcysteine solutions A1–F1 and A2–F2 using a Hg–S single scattering path, and their corresponding ^{199}Hg NMR chemical shifts ($C_{Hg(II)}$ ~ 100 mM; see Fig. 1 and 3)[a]

Solution (H_2NAC/Hg^{2+})	Hg–S			^{199}Hg NMR	Solution (H_2NAC/Hg^{2+})	Hg–S			^{199}Hg NMR
	N	R (Å)	σ^2 ($Å^2$)	δ (ppm)		N	R (Å)	σ^2 ($Å^2$)	δ (ppm)
pH = 7.5					pH = 10.5				
A1 (2.0)	2.0	2.33	0.0035	−924	A2 (2.0)	1.9	2.33	0.0029	−902
B1 (3.0)	1.9	2.34	0.0040	−758	B2 (3.0)	2.3	2.41	0.0067	−374
C1 (4.0)	2.0	2.35	0.0052	−645	C2 (4.0)	2.9	2.47	0.0102	−305
D1 (5.0)	2.0	2.36	0.0054	−570	D2 (5.0)	3.4	2.49	0.0107	−309
E1 (8.0)	2.4	2.37	0.0074	−521	E2 (8.0)	3.4	2.51	0.0084	−331
F1 (10.0)	2.5	2.39	0.0074	−495	F2 (10.0)	3.6	2.52	0.0081	−338

[a] Fitting k-range = 3.5–15.8 $Å^{-1}$ (except for F2, up to k = 13.0 $Å^{-1}$); S_0^2 = 0.9 fixed; estimated error limits: N ± 20%, R ± 0.02 Å, σ^2 ± 0.001 $Å^2$.

Table 4 EXAFS analyses of the relative amount of $Hg(NAC)_n$ species (n = 2, 3, 4) in solutions A1–F1 and A2–F2 (see also Table S1, Fig. S3a and b, ESI)[a]

Species Hg–S distance (Å)	% $Hg(NAC)_2^{2-}$ 2.33	% $Hg(NAC)_3^{4-}$ 2.42 (σ^2 = 0.004)	% $Hg(NAC)_4^{6-}$ 2.52	Average R^c	% $Hg(NAC)_2^{2-}$ 2.33	% $Hg(NAC)_3^{4-}$ 2.42 (σ^2 = 0.005)	% $Hg(NAC)_4^{6-}$ 2.52	Average R^c
A1 (2.0)[b]	100			2.330	100			2.330
B1 (3.0)	88	12		2.341	87	13		2.342
C1 (4.0)	72	28		2.355	68	32		2.359
D1 (5.0)	63	33	4	2.367	60	40		2.366
E1 (8.0)	49	40	11	2.387	45	48	7	2.387
F1 (10.0)	39	48	13	2.398	34	58	8	2.397
A2 (2.0)	100			2.330	100			2.330
B2 (3.0)	26	55	19	2.416	19	67	14	2.417
C2 (4.0)	9[d]	38	53	2.465	5[d]	45	50	2.466
D2 (5.0)	6[d]	29	65	2.480	2[d]	35	63	2.481
E2 (8.0)	4[d]	10	86	2.502	2[d]	12	86	2.504
F2 (10.0)		7	93	2.513		8	92	2.512

[a] Estimated accuracy is within ±10–15%; the left and right hand sides of this table show how the assumed σ^2 value for the HgS_3 complex (0.004 Å^2 and 0.005 Å^2, respectively) affects the relative amounts of the species. [b] Numbers in brackets refer to the $H_2NAC/Hg(II)$ mole ratio. [c] The average R = Σ(% of species) × (average Hg–S distance in the species) can be compared to the average distances obtained for solutions A1–F1 and A2–F2 (Table 3). [d] Not observed in Raman.

934 cm^{-1} unsuitable for internal calibration. The peak at 685 cm^{-1} is assigned as the C–S stretching in *N*-acetylcysteine.

^{199}Hg Nuclear Magnetic Resonance (NMR) spectroscopy

The ^{199}Hg NMR chemical shift can vary over a range of ~5000 ppm, and is very sensitive to the chemical environment around Hg(II) ions; *e.g.* the type and number of coordinating atoms, and also the solvent and temperature. The shielding effect of the ligand donor atoms is in the order: O > N > S.[30,38–41] The ^{199}Hg NMR chemical shifts for some selected Hg(II) thiolate complexes are listed in Table 5.

The NMR spectra of 0.1 M mercury(II) solutions with increasing amounts of *N*-acetylcysteine are shown in Fig. 3. Due to the fast ligand exchange equilibria between Hg(II) species present in the solution, only a single averaged resonance peak appears in each spectrum.

For solutions A1 and A2, both with the ligand to metal mole ratio $H_2NAC/Hg(II)$ = 2.0, the sharp signal with the ^{199}Hg chemical shift at around −900 ppm can be assigned to the dithiolate complex $Hg(NAC)_2^{2-}$ (Table 5). As the ligand concentration increases to C_{H_2NAC} = 0.3 M, the signal for solution B2 (pH 10.5) shows a sudden shift to −374 ppm, while the ^{199}Hg chemical shift for solution B1 (pH 7.5) with the same $H_2NAC/Hg(II)$ mole ratio appears at −758 ppm. Further increase in ligand concentration for solutions C1–F1 (pH 7.5) gradually shifts the signal downfield to −495 ppm, while for solutions C2–F2 (pH 10.5) the signal shows a minor upfield shift from −305 ppm to −338 ppm.

Discussion

Hg(II) *N*-acetylcysteine complex formation at pH 7.5

For solution A1 containing $C_{Hg(II)}$ = 0.1 M and C_{H_2NAC} = 0.2 M, the Hg–S bond distance 2.33 ± 0.01 Å obtained from EXAFS spectroscopy, the ^{199}Hg NMR signal at −924 ppm, and the symmetric S–Hg–S stretching Raman band at 332 cm^{-1} (Table 3; Fig. 2 and 3) are all consistent with a dominating linear Hg(II) dithiolate complex, $Hg(NAC)_2^{2-}$ (see Table 5). By increasing the total ligand concentration from 0.3 M in solution B1 to 1.0 M in solution F1, the average Hg–S bond distance increases from 2.34 to 2.39 ± 0.02 Å (Table 3), and the ^{199}Hg NMR signal shows a downfield shift from −758 to −495 ppm

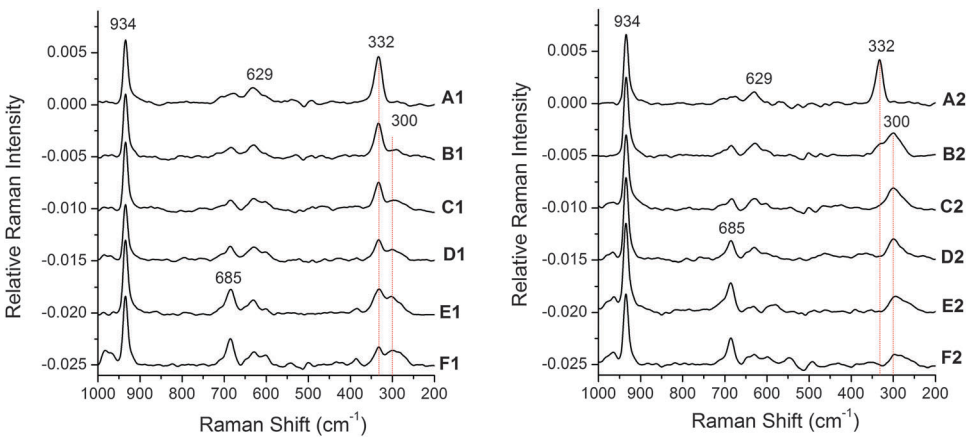

Fig. 2 Raman spectra of Hg(II) *N*-acetylcysteine solutions at physiological (A1–F1) and alkaline (A2–F2) pH, after baseline correction and smoothing.

Table 5 ^{199}Hg NMR chemical shifts for selected Hg(II) thiolates[a]

Coordination	^{199}Hg NMR chemical shift	Ref.
HgS_2	−1200 to −800 ppm $Hg(GS)_2$ (−960 to −993 ppm)	28–30, 42
HgS_2N_2	$Hg(Pen)_2^{2-}$ (−619 ppm), $Hg(Cys)_2^{2-}$ (−609 to −656 ppm) $Hg(SCH_2CH_2NH_2)_2$ (−608 ppm) Hg(II) substituted plastocyanin (−749 ppm; $HgSS'N_2$)	26–28, 36, 43, 44
HgS_3	*Aliphatic thiolates*: $Hg(S\text{-}i\text{-}Pr)_3^-$ (−79 ppm), $Hg(S\text{-}t\text{-}Bu)_3^-$ (−157 ppm), $Hg(GS)_3$ (∼−169 ppm)[b] Hg–MerR protein (−106 ppm) *Aromatic thiolates*: $Hg(SPh)_3^-$ (−341 to −354 ppm), $Hg(S\text{-}2,4,6\text{-}i\text{-}Pr_3C_6H_2)_3^-$ (−267 ppm)	28, 38, 39, 45
$HgS_3\cdots N_2$	$Hg(Pen)_3^{4-}$ (∼−390 ppm)[b]	27
HgS_4	*Aliphatic thiolates*: $Hg(SCH_3)_4^{2-}$ (−374 ppm), $Hg(SC_2H_5)_4^{2-}$ (−302 ppm) $Hg(S\text{-}i\text{-}Pr)_4^{2-}$ (−275 ppm), $Hg(Cys)_4^{6-}$ (∼−340 ppm)[b] *Aromatic thiolate*: $Hg(SC_6H_5)_4^{2-}$ (−585 ppm)	26, 30, 38, 46

[a] GSH = glutathione; MerR = metalloregulatory protein. [b] Estimated value.

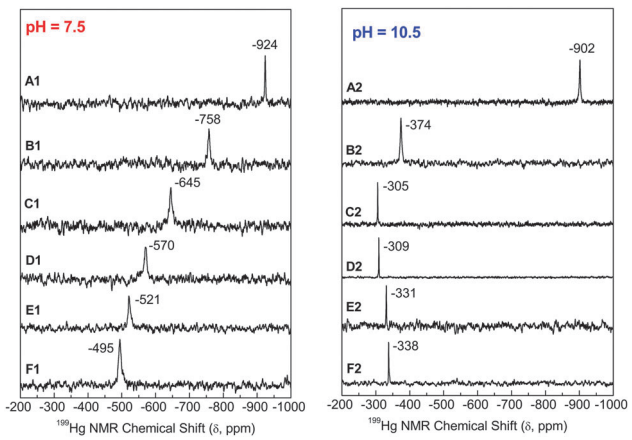

Fig. 3 ^{199}Hg NMR spectra of 0.1 M Hg(II) *N*-acetylcysteine solutions at physiological (A1–F1) and alkaline (A2–F2) pH.

(Fig. 3), while the intensity of the Raman band at 332 cm^{-1} is reduced (Fig. 2). Fitting the EXAFS spectra of these solutions to linear combinations of simulated EXAFS spectra shows a dominating linear $Hg(NAC)_2^{2-}$ complex in solutions B1–D1, while in solutions E1 and F1 with high ligand excess (H_2NAC/Hg(II) mole ratios 8 and 10, respectively) an almost equal mixture of $Hg(NAC)_2^{2-}$ and $Hg(NAC)_3^{4-}$ complexes and probably a minor amount (<10%) of the $Hg(NAC)_4^{6-}$ complex are present (see Table 4, Table S1 and Fig. S3a, ESI†). The best fit was obtained assuming a mean Hg–S distance of 2.42 ± 0.02 Å for the $Hg(NAC)_3^{4-}$ complex, which is comparable to that of the $Hg(glutathione)_3$ complex.[28] Also the relative intensities of the two Raman bands at 332 and 300 cm^{-1} (Fig. 2) provide experimental evidence for the mixture of $Hg(NAC)_2^{2-}$ and $Hg(NAC)_3^{4-}$ complexes. Previously, we observed for 0.1 M Hg(II) solutions with Cys/Hg(II) mole ratios 8 and 10 (pH 11), a broad Raman band at 277 cm^{-1}, which was deconvoluted into two peaks; the band at 285 cm^{-1} was assigned to ν_{sym}(Hg–S) for the $Hg(Cys)_3^{4-}$ complex, with an estimated mean Hg–S distance of 2.44 ± 0.02 Å.[26] The slightly shorter mean Hg–S distance (2.42 ± 0.02 Å) for the $Hg(NAC)_3^{4-}$ complex is consistent with a somewhat stronger Hg–S bond for the higher frequency ν_{sym}(Hg–S) = 300 cm^{-1}, assuming similar effective ligand mass. For the Hg(II)–MerR complex (MerR = metalloregulatory protein) with trigonal HgS_3 coordination of cysteine residuals, a symmetric Hg–S stretching band at 282 cm^{-1} has been reported.[47]

Hg(II) *N*-acetylcysteine complex formation at pH 10.5

The structural and spectroscopic information obtained for the alkaline aqueous solution A2 with the H_2NAC/Hg(II) mole ratio 2.0, *i.e.* the mean Hg–S distance 2.33 ± 0.01 Å, $\delta(^{199}Hg)$ = −902 ppm, and the symmetric S–Hg–S stretching at 332 cm^{-1} (Table 3; Fig. 2 and 3), indicates a dominating $Hg(NAC)_2^{2-}$ complex, as for solution A1 (pH 7.5). At pH = 10.5, *N*-acetylcysteine is completely deprotonated to NAC^{2-} (Fig. S1, ESI†), promoting formation of the higher complexes $Hg(NAC)_3^{4-}$ and $Hg(NAC)_4^{6-}$ at much lower total ligand concentration, as *e.g.* by increasing C_{H_2NAC} from 0.2 M in solution A2 to 0.3 M in B2 (Table 4). The formation of a dominating $Hg(NAC)_3^{4-}$ complex is evidenced by a sudden increase in the average Hg–S distance to 2.41 ± 0.02 Å, a sudden downfield shift of $\delta(^{199}Hg)$ to −374 ppm, and a loss of intensity for the Raman band at 332 cm^{-1}, while the band at 300 cm^{-1} assigned to the tri-thiolate complex $Hg(NAC)_3^{4-}$ gains intensity (Table 3; Fig. 2 and 3). Those variations are much more drastic than for the solutions A1–F1 series (see above), since at pH 7.5 less than 3% of the free ligand is in the NAC^{2-} form with the deprotonated thiol group (Fig. S1, ESI†). For example, solution B1 (pH 7.5) with similar total ligand and metal concentrations to B2 shows an average Hg–S distance of 2.34 ± 0.02 Å and mainly contains the linear $Hg(NAC)_2^{2-}$ complex.

By increasing the total ligand concentration in solutions C2–F2, the vibrational band at 332 cm^{-1} for the $Hg(NAC)_2^{2-}$ complex disappears, the intensity of the Raman band at 300 cm^{-1}, and therefore the amount of $Hg(NAC)_3^{4-}$ complex gradually decrease, while the ^{199}Hg NMR signal shows a minor upfield shift from −305 ppm in C2 to −338 ppm in F2. A useful

parameter for describing the changes in chemical composition for these solutions is the average Hg–S distance, which increases from 2.47 to 2.52 ± 0.02 Å, when C_{H_2NAC} is raised from 0.4 M (C2) to 1.0 M (F2). When comparing solutions F1 (pH 7.5) and F2 (pH 10.5), both containing $C_{Hg(II)}$ = 0.1 M and C_{H_2NAC} = 1.0 M, the mean Hg–S distance for solution F2 with much higher free thiolate concentration is considerably higher than that of solution F1 (2.39 ± 0.02 Å). Fitting the EXAFS spectra of these solutions to linear combinations of simulated EXAFS oscillations shows that 80–90% of Hg(II) ions in solution F2 are in the form of $Hg(NAC)_4^{6-}$ species with a mean Hg–S distance of 2.52–2.53 Å; this is the first report of a tetrathiolate Hg(II) *N*-acetylcysteine species.

Considering the observed chemical shifts in the ^{199}Hg NMR spectra of solutions B1–F1 and A2–F2, and the approximate percentage of di-, tri- and tetrathiolate Hg(II) complexes in these solutions (Table 4 and Table S1, ESI†), the ^{199}Hg NMR chemical shifts for the $Hg(NAC)_3^{4-}$ and $Hg(NAC)_4^{6-}$ species can be estimated to be about −170 and −350 ppm, respectively. These values are in close agreement with our previously proposed chemical shift values δ(Hg) ∼ −169 ppm for $Hg(GS)_3^{7-}$,[28] (GS = deprotonated form of glutathione), and δ(Hg) ∼ −340 ppm for $Hg(Cys)_4^{6-}$.[26]

Hg(II) complex formation with cysteine, *N*-acetylcysteine and penicillamine at alkaline pH

Fig. 4 compares the variations in average Hg–S distances, and also ^{199}Hg NMR chemical shifts, for the Hg(II) alkaline aqueous solutions each containing cysteine, *N*-acetylcysteine or penicillamine, as a function of total ligand concentration. At low total ligand concentration, both cysteine and penicillamine mainly form $Hg(N,S\text{-Cys})_2^{2-}$ and $Hg(N,S\text{-Pen})_2^{2-}$ complexes (Hg–S 2.34 ± 0.02 Å, Hg–N 2.52–2.56 Å, δ_{Hg} = −609 to −619 ppm), while *N*-acetylcysteine forms $Hg(S\text{-NAC})_2^{2-}$ (Hg–S 2.33 ± 0.01 Å, δ_{Hg} = −902 ppm). The highest amount of trithiolate complex is observed already at the mole ratio C_{H_2NAC}/Hg(II) = 3 for *N*-acetylcysteine: $Hg(S\text{-NAC})_3^{4-}$ (Hg–S 2.42 ± 0.02 Å, δ_{Hg} ∼ −170 ppm), and at the mole ratio C_{H_2Cys}/Hg(II) = 4 for cysteine: $Hg(S\text{-Cys})_3^{4-}$ (Hg–S 2.44 ± 0.02 Å). In an excess amount of free thiolate, both cysteine and *N*-acetylcysteine mainly form tetrathiolate complexes, $Hg(S\text{-Cys})_4^{6-}$ and $Hg(S\text{-NAC})_4^{6-}$, with the mean Hg–S bond distance 2.52 ± 0.02 Å, δ_{Hg} ∼ −340 to −350 ppm,[26] while penicillamine forms a $Hg(Pen)_3^{4-}$ complex (Hg–S 2.44 ± 0.02 Å, δ_{Hg} ∼ −390 ppm) with the HgS_3 core weakly interacting with two amine groups.[27]

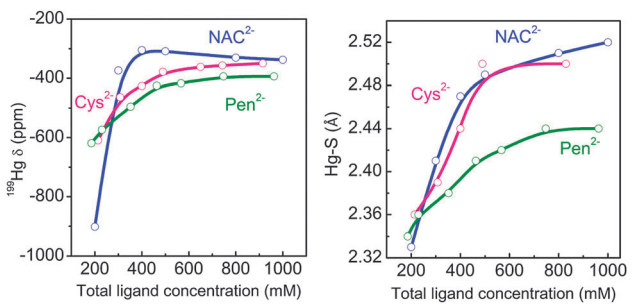

Fig. 4 Comparison between ^{199}Hg NMR chemical shift variations and mean Hg–S distances *vs.* total ligand concentration for 0.1 M Hg(II) alkaline aqueous solutions containing cysteine, penicillamine or *N*-acetylcysteine.

Conclusion

The current study shows that both at physiological and alkaline pH, the Hg(II) ion forms a linear $Hg(NAC)_2^{2-}$ complex with *N*-acetylcysteine at the H_2NAC/Hg(II) mole ratio 2.0. For this complex the Hg–S bond distance is 2.33 ± 0.01 Å, with a symmetric S–Hg–S stretching Raman band at 332 cm^{-1} and a ^{199}Hg NMR chemical shift above −900 ppm. In ligand excess, a mixture of $Hg(NAC)_2^{2-}$ and $Hg(NAC)_3^{4-}$ species predominate at physiological pH, while at alkaline pH, the high free thiolate concentration shifts the equilibria toward formation of the tetrathiolate $Hg(NAC)_4^{6-}$ complex, reported here for the first time (see Scheme 2). The average Hg–S bond distances for the tri- and tetra-thiolate $Hg(NAC)_3^{4-}$ and $Hg(NAC)_4^{6-}$ species are 2.42 ± 0.02 Å and 2.52 ± 0.02 Å, with estimated ^{199}Hg chemical shifts of ∼−170 and −350 ppm, respectively.

Based on this structural information, *N*-acetylcysteine shows similar behavior toward Hg(II) ions at physiological pH as glutathione,[29] metalloregulatory (MerR) protein,[48] and metallothioneins (MT),[49,50] and should be capable of acting as an antidote toward inorganic mercury(II).

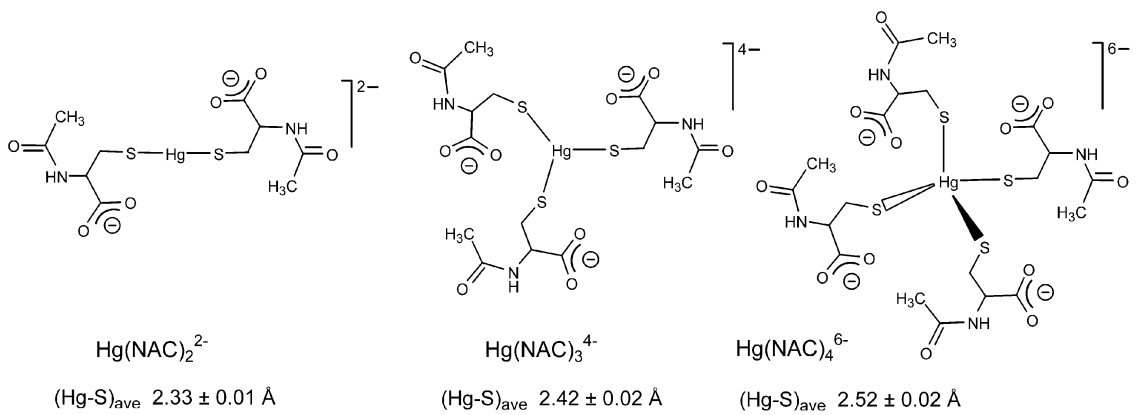

Scheme 2 Proposed structures for the Hg(II) *N*-acetylcysteine complexes; $Hg(NAC)_2^{2-}$ and $Hg(NAC)_3^{4-}$ formed at physiological pH.

In alkaline media both cysteine and *N*-acetylcysteine, when present in excess, tend to form tetrathiolate complexes with Hg(II) ions. Penicillamine, as a result of the steric hindrance created by its methyl groups, only forms a trithiolate Hg(II) complex under similar conditions. At low L/Hg(II) mole ratios ($\sim$2–3), the amino coordination in the stable Hg(*N*,*S*-Cys)$_2^{2-}$ and Hg(*N*,*S*-Pen)$_2^{2-}$ chelates creates an additional resistance toward addition of another thiolate group, while for *N*-acetylcysteine with a blocked amine group, formation of higher complexes is easier.

Acknowledgements

We are grateful to Dr Michelle Foregeron, Qiao Wu and Dorothy Fox, at the instrument facility at the Department of Chemistry, for their constant support and skillful assistance in measuring the NMR spectra. X-ray absorption measurements were carried out at the Stanford Synchrotron Radiation Lightsource (SSRL), which is operated by the Department of Energy, Office of Basic Energy Sciences, USA. The SSRL Biotechnology Program is supported by the National Institutes of Health, National Center for Research Resources, Biomedical Technology Program, and by the Department of Energy, Office of Biological and Environmental Research (proposal numbers 3391 and 3637). We gratefully acknowledge the Natural Sciences and Engineering Council (NSERC) of Canada, Canadian Foundation for Innovation (CFI) and Alberta Science and Research Investment Program (ASRIP) for providing financial support.

References

1 T. W. Clarkson, *Environ. Health Perspect.*, 2002, **110**(suppl. 1), 11–23.
2 T. W. Clarkson and L. Magos, *Crit. Rev. Toxicol.*, 2006, **36**, 609–662.
3 M. Korbas, T. C. MacDonald, I. J. Pickering, G. N. George and P. H. Krone, *ACS Chem. Biol.*, 2012, **7**, 411–420.
4 M. Korbas, J. L. O'Donoghue, G. E. Watson, I. J. Pickering, S. P. Singh, G. J. Myers, T. W. Clarkson and G. N. George, *ACS Chem. Neurosci.*, 2010, **1**, 810–818.
5 M. Blanusa, V. M. Varnai, M. Piasek and K. Kostial, *Curr. Med. Chem.*, 2005, **12**, 2771–2794.
6 G. Guzzi and C. A. M. La Porta, *Toxicology*, 2008, **244**, 1–12.
7 M. Zafarullah, W. Q. Li, J. Sylvester and M. Ahmad, *Cell. Mol. Life Sci.*, 2003, **60**, 6–20.
8 Anonymous, *Altern. Med. Rev.*, 2000, **5**, 467–471.
9 G. S. Kelly, *Altern. Med. Rev.*, 1998, **3**, 114–127.
10 W. A. Watson, T. L. Litovitz, W. Klein-Schwartz, G. C. Rodgers Jr, J. Youniss, N. Reid, W. G. Rouse, R. S. Rembert and D. Borys, *Am. J. Emerg. Med.*, 2004, **22**, 335–404.
11 N. Ballatori, M. W. Lieberman and W. Wang, *Environ. Health Perspect.*, 1998, **106**, 267–271.
12 M. E. Lund, W. Banner, W. C. Thomas and M. Berlin, *J. Clin. Toxicol.*, 1984, **22**, 31–49.
13 H. Ottenwalder and P. Simon, *Arch. Toxicol.*, 1987, **60**, 401–402.
14 G. Girardi and M. M. Elias, *Toxicology*, 1991, **67**, 155–164.
15 S. Truempler, S. Nowak, B. Meermann, G. Wiesmueller, W. Buscher, M. Sperling and U. Karst, *Anal. Bioanal. Chem.*, 2009, **395**, 1929–1935.
16 A. Becker and K. A. Soliman, *Neurochem. Res.*, 2009, **34**, 1677–1684.
17 J. K. Kim, M. Han and M. Nili, *Chemosphere*, 2011, **85**, 1635–1638.
18 R. K. Zalups and S. Ahmad, *J. Pharmacol. Exp. Ther.*, 2005, **314**, 1158–1168.
19 M. S. Madejczyk, D. A. Aremu, T. A. Simmons-Willis, T. W. Clarkson and N. Ballatori, *J. Pharmacol. Exp. Ther.*, 2007, **322**, 378–384.
20 R. Brandão, F. W. Santos, G. Zeni, J. B. Rocha and C. W. Nogueira, *Biometals*, 2006, **19**, 389–398.
21 R. Brandão and C. W. Nogueira, *Food Chem. Toxicol.*, 2010, **49**, 305–308.
22 F. M. Rubino, C. Verduci, R. Giampiccolo, S. Pulvirenti, G. Brambilla and A. Colombi, *J. Am. Soc. Mass Spectrom.*, 2004, **15**, 288–300.
23 B. Noszal, D. Visky and M. Kraszni, *J. Med. Chem.*, 2000, **43**, 2176–2182.
24 H. Kõszegi-Szala, T. L. Paál and L. Barcza, *Z. Physiol. Chem.*, 2000, **214**, 45–54.
25 M. A. Basinger, J. S. Casas, M. M. Jones, A. D. Weaver and N. H. Weinstein, *J. Inorg. Nucl. Chem.*, 1981, **43**, 1419–1425.
26 F. Jalilehvand, B. O. Leung, M. Izadifard and E. Damian, *Inorg. Chem.*, 2006, **45**, 66–73.
27 B. O. Leung, F. Jalilehvand and V. Mah, *Dalton Trans.*, 2007, 4666–4674.
28 V. Mah and F. Jalilehvand, *JBIC, J. Biol. Inorg. Chem.*, 2008, **13**, 541–553.
29 V. Mah and F. Jalilehvand, *Chem. Res. Toxicol.*, 2010, **23**, 1815–1823.
30 J. G. Wright, M. J. Natan, F. M. MacDonnell, D. M. Ralston and T. V. O'Halloran, *Prog. Inorg. Chem.*, 1990, **38**, 323–412.
31 G. Klose, F. Volke, G. Peinel and G. Knobloch, *Magn. Reson. Chem.*, 1993, **31**, 548–551.
32 G. N. George, S. J. George and I. J. Pickering, *EXAFSPAK*, Stanford Synchrotron Radiation Lightsource (SSRL), Menlo Park, CA, 2001.
33 T. Ressler, *J. Synchrotron Radiat.*, 1998, **5**, 118–122.
34 S. I. Zabinsky, J. J. Rehr, A. Ankudinov, R. C. Albers and M. J. Eller, *Phys. Rev. B: Condens. Matter Mater. Phys.*, 1995, **52**, 2995.
35 A. L. Ankudinov and J. J. Rehr, *Phys. Rev. B: Condens. Matter Mater. Phys.*, 1997, **56**, R1712.
36 H. Fleischer, Y. Dienes, B. Mathiasch, V. Schmitt and D. Schollmeyer, *Inorg. Chem.*, 2005, **44**, 8087–8096.
37 J. W. Nebgen, A. D. McElroy and H. F. Klodowski, *Inorg. Chem.*, 1965, **4**, 1796–1799.
38 G. A. Bowmaker, R. K. Harris and S.-W. Oh, *Coord. Chem. Rev.*, 1997, **167**, 49–94.
39 L. M. Utschig, J. W. Bryson and T. V. O'Halloran, *Science*, 1995, **268**, 380–385.

40 D. L. Huffman, L. M. Utschig and T. V. O'Halloran, *Met. Ions Biol. Syst.*, 1997, **34**, 503–526.
41 G. Öz, D. L. Pountney and I. M. Armitage, *Biochem. Cell Biol.*, 1998, **76**, 223–234.
42 J. L. Sudmeier, R. R. Birge and T. G. Perkins, *J. Magn. Reson.*, 1978, **30**, 491–496.
43 L. M. Utschig, J. G. Wright, G. Dieckmann, V. Pecoraro and T. V. O'Halloran, *Inorg. Chem.*, 1995, **34**, 2497–2498.
44 L. M. Utschig, T. Baynard, C. Strong and T. V. O'Halloran, *Inorg. Chem.*, 1997, **36**, 2926–2927.
45 M. J. Natan, C. F. Millikan, J. G. Wright and T. V. O'Halloran, *J. Am. Chem. Soc.*, 1990, **112**, 3255–3257.
46 G. K. Carson and P. A. W. Dean, *Inorg. Chim. Acta*, 1982, **66**, 157–161.
47 G. Fleissner, P. M. Kozlowski, M. r. Vargek, J. W. Bryson, T. V. O'Halloran and T. G. Spiro, *Inorg. Chem.*, 1999, **38**, 3523–3528.
48 J. G. Wright, H. T. Tsang, J. E. Penner-Hahn and T. V. O'Halloran, *J. Am. Chem. Soc.*, 1990, **112**, 2434–2435.
49 D. T. Jiang, S. M. Heald, T. K. Sham and M. J. Stillman, *J. Am. Chem. Soc.*, 1994, **116**, 11004–11013.
50 S. S. Hasnain, in *Synchrotron Radiation in Chemistry and Biology II*, ed. E. Mandelkow, Springer, Berlin, Heidelberg, 1988, vol. 147, pp. 73–93.

